Journal of the European Ceramic Society 22 (2002) 567–572

www.elsevier.com/locate/jeurceramsoc

Crystal structure, electrical conductivity and Seebeck coefficient of $Y(Mn,Ni)O_3$ solid solution

D. Gutierrez[a], O. Peña[b], P. Duran[a], C. Moure[a,*]

[a]*Instituto de Ceramica y Vidrio, CSIC, Electroceramics Department, 28500 Arganda, Madrid, Spain*
[b]*LCSIM/UMR6511-CNRS, Université de Rennes I, Rennes, France*

Received 20 January 2001; received in revised form 18 April 2001; accepted 28 April 2001

Abstract

Solid solutions belonging to the Mn-rich region of the $YNi_xMn_{1-x}O_3$ system have been studied. The powders were prepared by solid state reaction between the corresponding oxides. Sintered ceramics were obtained by firing at 1325–1350°C. The incorporation of 20 at.% Ni^{2+} to the yttrium manganite induces the formation of a perovskite-type phase, with orthorhombic symmetry and space group Pbmn. Increase of the Ni amount leads to an increase of the orthorhombicity factor b/a of the perovskite, up to an amount of 50 at.% Ni^{2+}. Above this Ni amount, a biphasic system has been observed, with the presence of unreacted Y_2O_3. DC electrical conductivity measurement has shown semiconducting behaviour for this solid solution with perovskite-type structure. The room temperature conductivity increases with Ni up to ~33 at.% Ni, and then decreases. Small polaron hopping mechanism controls the conductivity in these ceramics. Results are discussed as a function of the Mn^{3+}/Mn^{4+} ratio for each composition. NTC thermistor capability and potential application as ceramic electrode for SOFCs are presented.

Keywords: Crystal structure; Electrical conductivity; Electrical properties; Perovskites; $Y(Mn,Ni)O_3$

1. Introduction

The rare earth (RE) manganites have attracted a great interest because of their electrical and magnetic properties such as their semiconducting behaviour and their magnetoresistive features. A lot of work has been developed about the properties of light RE manganites, particularly on the knowledge of the features of the $LaMnO_3$ compound, modified by Sr or Ca substitution.[1,2] Use of these solid solutions as ceramic electrodes for solid oxide fuel cells (SOFCs) is being studied from several years ago.[3] Recently, the colossal magnetoresistive effect found in both single crystals and bulk ceramic of those solid solutions has been extensively treated by many authors.[4]

The light RE manganites crystallise with a perovskite-type structure and space group (SG) Pbmn, which tends to increase its anisotropy when the atomic weight of the RE element increases, and its ionic radius decreases, from rhombohedral, quasi-cubic symmetry for La, to orthorhombic symmetry, for Dy with high b/a ratio. For ions such as Er and smaller the RE manganites crystallise with a hexagonal symmetry and SG P63cm[5] despite the corresponding values of the Goldschmidt tolerance factor $t = (r_A + r_O)/(r_B + r_O)^*\sqrt{2}$ for the perovskite structure. The structural change from perovskite-type to hexagonal symmetry can be associated not only to the decrease of the tolerance factor but also to the presence of a Jahn–Teller-type Mn^{3+} cation on B sites with octahedral co-ordination. Such a cation promotes a strong anisotropic deformation, which induces the change of symmetry, when the tolerance factor attains an enough small value.[6] In contrast, the heavy RE ferrites, such as the $ErFeO_3$ with the same tolerance factor, ~0.80, as of $ErMnO_3$, crystallises with an orthorhombic perovskite-type structure.

The $YMnO_3$ is a ferroelectric, antiferromagnetic compound with a very low value of electrical conductivity.[7] At high voltages it shows a peculiar non-ohmic behaviour.[8] Its solid solution with the $CaMnO_3$ perovskite shows a transition to this latter structure for an amount of approximately 22 at.% of Ca. These solid solutions are semiconducting compounds, and the activation energy for conduction decreases to very low

* Corresponding author. Tel.: +34-91-871-1800; fax: +34-91-870-0550.
E-mail address: cmoure@icv.csic.es (C. Moure).

0955-2219/02/$ - see front matter
PII: S0955-2219(01)00302-8

values, with a subsequent rise of the conductivity values when the Ca amount raises.[9] This fact makes it possible to use these solid solutions as ceramic electrode for SOFCs.

On the other hand, there is little work about the modification of the $YMnO_3$ by incorporation of appropriate cations on the Mn sublattice. The scope of the present work is to study the effect of the incorporation of Ni^{2+} cations on the structure, symmetry and electrical properties of the $YMnO_3$.

2. Experimental methods

$Y(Ni_xMn_{1-x})O_3$ compositions with $x = 0.10-0.55$, were prepared by solid state reaction between stoichiometric mixtures of MnO, NiO, and Y_2O_3 reagent grade oxides as raw materials with submicronic particle size. The mixtures were homogenised by wet attrition milling, using isopropanol as liquid medium. The dried mixtures were calcined at 1000°C for 2 h. The calcined cakes were remilled by the same technique, dried, granulated, and uniaxially pressed. Granulometric analysis was carried out on the synthesised powders by means of laser counting, (Mastersizer model, Malvern Instruments, Ltd, UK) and BET techniques, (Quantachrome MS-16 model, Syosset, NY, USA). The pressed pellets were sintered between 1300 and 1400°C for 2 h, and at 1325°C for several times from 1 to 8 h. Apparent density was measured by water displacement. XRD analysis was performed both on the calcined powder and on the sintered samples using a D-5000 Siemens Diffractometer and CuK_α radiation. The powder was identified by scanning at a rate of 2° 2θ/min, and the lattice parameters were calculated from the spectra obtained on the sintered samples at a scanning rate of $\frac{1}{2}$° 2θ/min. Powder of Si was employed as an internal standard. The microstructure of the sintered ceramics was observed by scanning electron microscopy (SEM), (Zeiss DSM 950, Oberkochem, Germany) on polished and thermally etched surfaces, and on fresh fracture surfaces. Disc-shaped samples were painted with silver paste and fired at 800°C, for 1 h. Four-points DC conductivity measurements were carried out for all the solid solutions with perovskite-type structure, between 20 and 700°C. For the measurements a Constant Current DC power supply (Tektronix, model PS280) and a HP Multimeter (model 44201[a]), with 1 μA DC current resolution were used. Activation energies were calculated from the corresponding Arrhenius plots. Curves ρ vs T were depicted for determining the NTC thermistor parameters. The Seebeck–Coefficient measurements were made on cylindrical samples 0.3 cm in diameter and 1.5 cm long, using almost the conventional technique for a rapid and qualitative determination of the majority charge-carrier sign.[10] For the measurements, the sample was held by two metal blocks containing the thermocouples. A heater on one block produced the temperature gradient in the sample. The thermoelectric voltage was measured between the same reference points.

The Goldschmidt tolerance factor t has been calculated using the ionic radii tabulated by Shannon,[11] taking into account the oxygen co-ordination of the involved cations and the existence of different valence states of the Mn, with different ionic radii, in the solid solutions. Mean ionic radius on A and B lattice sites has been used when two or more cations are present on that sites.

3. Results and discussion

The apparent particle size, as measured by laser counting was 1 μm, but this size corresponds to that of aggregates. The BET measurements indicated specific surface area values of 4 m^2/g, which correlates well with an average particle size of ~0.2 μm.

Fig. 1 shows the corresponding curves of apparent density vs temperature and vs time of perovskite-type samples, $x = 0.20-0.50$. It can be seen that the maximum apparent density values for several compositions were obtained at 1325°C, for 2 h, with values ranging from 94 to 96% of the theoretical density (D_{th}). Fig. 2 depicts the microstructure of a sintered sample. Small grain size is the most characteristic feature of the microstructure of all the studied samples.

The XRD phase analysis of the sintered bodies is shown in Fig. 3. As it can be seen from these diffractograms, for Ni amounts of 40 at.%, the phase which is forming is a perovskite-type phase. Above 50 at.% Ni, a different pattern can be seen with the appearance of unreacted Y_2O_3.

Table 1 resumes the measured values of the lattice parameters as a function of the Ni content. Formation of a perovskite-type phase was observed for Ni amounts ranging from 10 to 50 at.% Ni^{2+}. For compositions containing an amount lower than 20 at.% Ni, biphasic samples were obtained. In those samples a main phase with hexagonal, $YMnO_3$-type structure was observed, along with small amounts of a perovskite-type phase, which grows with the Ni amount. For samples containing 20 to 50 at.% Ni, a single phase was identified. This phase was indexed as an orthorhombic perovskite-type compound, isomorphous to $GdMnO_3$ and with a S.G. Pbnm. As it can be seen in the Table 1, the orthorhombicity of the perovskite phases increases with the Ni amount. Above 50 at.% Ni, the samples showed two phases again, coexisting the perovskite phase with unreacted Y_2O_3. The lattice parameters of the perovskite corresponding to the composition with 55 at.% Ni, not shown in the Table 1, are the same of that corresponding to the 50/50 composition. These results seem to indicate that the Ni cannot take a valence state of 3+. Therefore,

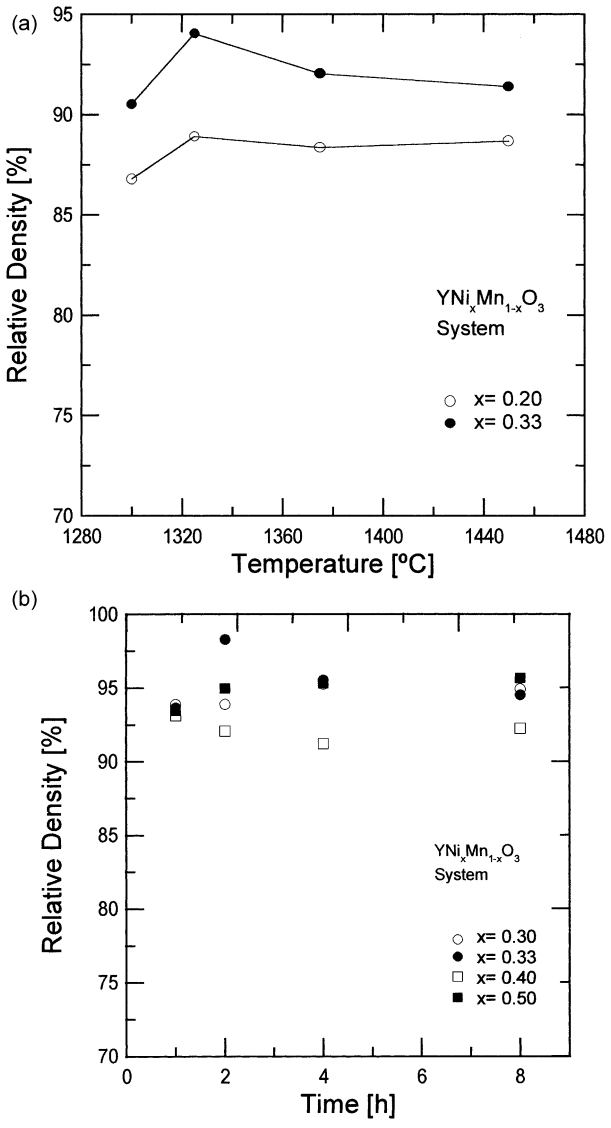

Fig. 1. (a) Relative density of the sintered samples as a function of the temperature at 2 h dwell time; and (b) as a function of time at constant temperature of 1325°C.

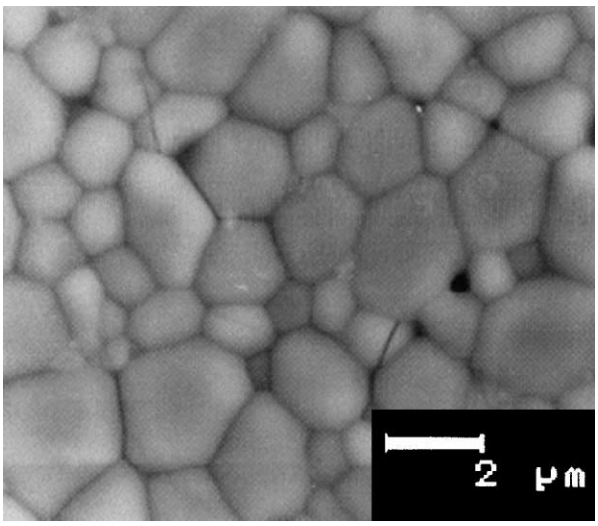

Fig. 2. Micrograph of polished and thermally etched surface of a sintered sample corresponding to the composition with 33 at.% Ni, sintered at 1325°C, 2 h.

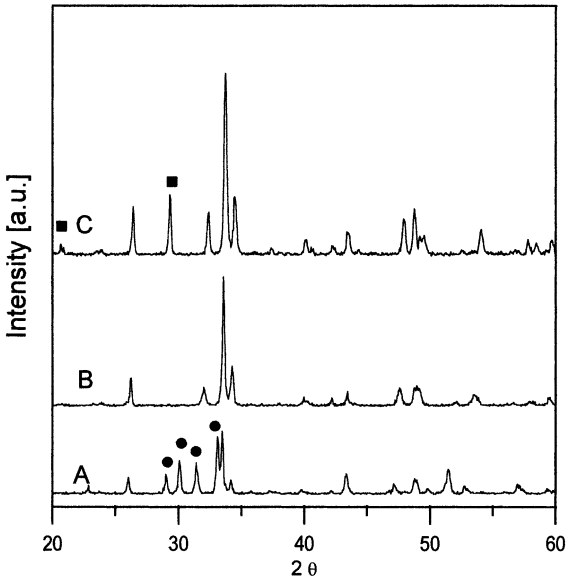

Fig. 3. XRD patterns of the solid solutions corresponding to samples with (A) 10, (B) 40 and (C) 55 at.% Ni; ● $YMnO_3$; ■ Y_2O_3.

it seems to be non-feasible to form a perovskite structure with the following ion distribution: $Y[Ni^{2+}_{0.45}Mn^{4+}_{0.45}Ni^{3+}_{0.10}]O_3$, and that the 50/50 composition is the boundary between a monophasic field and a new biphasic field.

The crystal chemistry behaviour of the samples containing $\leqslant 50$ at.% Ni is very similar to that observed in other systems, such as $(Y,Ca)MnO_3$, $(Er,Ca)MnO_3$ and $(Gd,Ca)MnO_3$.[12]

The progressive disappearance of the Jahn–Teller cations, Mn^{3+}, which are changing to the 4+ valence state, because of the incorporation of lower-valence state cations such as the Ni^{2+} for compensating charges, decreases the high anisotropy of the crystalline lattice. This decrease promotes the appearance of a perovskite-type phase. When the orthorhombicity of these solid solutions and that of the $GdMnO_3$ compound[12] are compared it is possible to appreciate that the b/a ratio of all those solid solutions is always lower than that of the pure Gd perovskite. Nevertheless, the tolerance factor t of these structures is lower than that of the mentioned Gd perovskite (Fig. 4), i.e. the factor t is not responsible for the lowering of b/a. For the $(Y,Ca)MnO_3$ solid solution, the tolerance factor increases with the Ca^{2+} content, due to the larger ionic radius of this cation against that of the Y^{3+}. This leads to an increase of the mean ionic radius on the A sites and therefore to an increase of t, in spite of the decrease of the mean ionic radius on the B sites caused by the appearance of the Mn^{4+} cation. On the contrary, in the solid solution of the present case, the tolerance factor remains practically unchanged. On the

Table 1
Lattice parameters of the solid solution $Y(Ni_xMn_{1-x})O_3$

At.% Ni	a (nm) (±0.0001)	b (nm) (±0.0001)	c (nm) (±0.0001)	b/a	V (nm^3) (±0.0004)	D_{th} (g/cm^3)
0[a]	0.6136	–	1.1400	–	0.3717	5.15
10[b]	0.5244	0.5677	0.7443	1.0826	0.2216	5.76
20	0.5243	0.5651	0.7460	1.0778	0.2211	5.79
30	0.5241	0.5638	0.7452	1.0757	0.2202	5.82
33	0.5239	0.5641	0.7449	1.0767	0.2202	5.83
40	0.5229	0.5656	0.7427	1.0816	0.2196	5.85
45	0.5223	0.5666	0.7414	1.0848	0.2194	5.86
50	0.5221	0.5667	0.7412	1.0854	0.2193	5.87

[a] Hexagonal lattice, $Z = 6$.
[b] Coexisting with hexagonal $YMnO_3$.

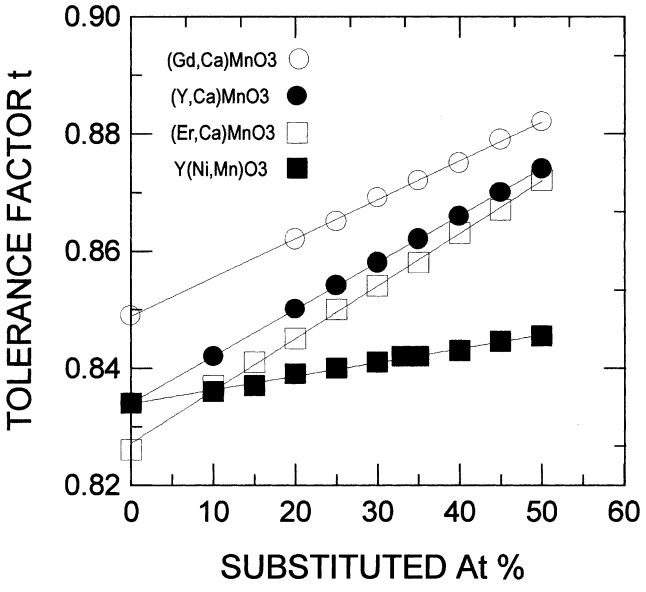

Fig. 4. Variation of tolerance factor t against substituting cation for several perovskite solid solutions.

other hand, the ionic radius of the Ni^{2+} is slightly larger than that of the Mn^{3+}, and therefore it could cause a decrease of the t value. This decrease can be compensated by the presence of Mn^{4+} cations. Therefore the reason for the change to the perovskite-type structure can only be attributed to the progressive disappearance of the Jahn–Teller cations, and not to a modification of the tolerance factor. The constancy of the t value can be the reason of the behaviour of the b/a ratio, with a very small decrease for values between 20 and 30 at.% and a subsequent increase from 33 to 50 at.%. The compactness grade of the perovskite lattice rises and the XRD density do it when the Ni^{2+} content increases.

When the data obtained in this system are compared with those existing in the literature, such as the above cited: (Y, Ca)MnO_3, and (Er,Ca)MnO_3[12] systems, it can be stated that the change from hexagonal to perovskite structure occurs at practically the same amount of the substituting cation, i.e. when the Mn^{3+} amount decreases below a critical value. This value is around 80 at.% of the Mn^{3+} original amount, independently of the value of the corresponding tolerance factor for stabilising the perovskite lattice. According to these results, it is possible to postulate the following general formula for the solid solution:

$$Y\left[Ni_x^{2+}Mn_x^{4+}Mi_{1-2x}^{3+}\right]O_3 \quad x = 0.20-0.50 \tag{1}$$

to maintain the equilibrium valence.

Fig. 5 shows the σT vs $1/T$ curves for compositions with $x = 0.30-0.50$. From this figure a feature is noticeable: The conductivity increases from 30 to 33 atomic percent Ni, and decreases from 40–50 at.% Ni. The reason of this behaviour could be attributed to the nature of the substituting cations. The Ni^{2+} seems not to contribute to the controlled valence conduction mechanism, because of the lack of another valence state of Ni^{2+} in the nearest neighbour sites. Therefore, the only pairs contributing to the conduction mechanism seem to be the Mn^{3+}–Mn^{4+} ones. It is easy to see that these possible pairs are increasing until an amount of 33 at.% Ni and 67 at.% Mn. A subsequent rise in the Ni percentage leads to a decrease of the possible forming pairs; it is possible to form 0.30 pairs per formula unit in the 30/70 composition. The number of pairs grows until 0.33 for 33/67 composition, whereas it is possible to form only 0.2 in the 40/60 composition, and 0.1 in the 45/55 one. This variation in the relative percentage between the two Mn cations explains the existence of a maximum in the conductivity values for an intermediate Ni percentage. The 50/50 composition has a theoretical formula $Y[Ni_{050}^{2+}Mn_{0.50}^{4+}]O_3$ in which no conducting mechanism seems to be possible. Nevertheless, this composition has shown semiconducting behaviour. The reason for such a behaviour could be related to the oxygen pick up process during the cooling of the ceramic samples. At the sintering temperatures, the most stable valences of Mn are $+3$ and $+2$. It is during the cooling when valence state $+4$ can be attained. The oxygen diffusion progress quickly by the grain boundary path but do it more slowly by bulk. The high density of the

samples could be responsible of the lack of a complete oxidation, in a similar manner to that occurring in YBaCuO superconductors.[14] The presence of residual Mn^{3+} could bring about the persisting semiconducting behaviour. More detailed study could be necessary to corroborate this assertion.

According to the results shown in Fig. 5, in which a linear relation between $\log(\sigma T)$ vs $1/T$ is observed, it can be established that the conductivity mechanism for these solid solutions is a thermally activated small polaron hopping, in a similar manner as other manganite-based ceramic semiconductors.[15]

Table 2 shows the room temperature conductivity values and the activation energy for electrical conduction of the single-phase samples. It can be seen that the conductivity values at 700°C for $Ni \leqslant 0.33$ are of the same order of magnitude than those corresponding to the more conventional ceramic electrodes for SOFCs.[13]

Fig. 6 shows the Seebeck coefficients of the solid solution. Measured values correlate well with the proposed semiconduction mechanism of small polaron hopping. Typical values of 80 μV/°C have been determined. It is possible to see that the sign of charge carriers changes when the Ni amount is higher than 40 at.%. This fact corroborates the above statement about the contribution of only Mn^{3+}–Mn^{4+} pairs to semiconducting mechanism. The samples with $Ni \leqslant 0.40$ have a percentage of Mn^{3+} higher than that of Mn^{4+}, according to the formula.[1] Therefore, the predominant charge carriers are holes. For $Ni \geqslant 0.40$, Mn^{4+} is higher than the Mn^{3+} amount. As consequence, the predominant carriers must be electrons. The behaviour observed for the composition 40/60 can be attributed to the above mentioned incomplete oxidation process, which makes that the change of the sign of the charge carriers, caused by the Mn^{3+}/Mn^{4+} ratio evolution, may be displaced to higher Ni/Mn ratios.

Fig. 7 displays the $\rho - T$ curves, coresponding to the 40, 45, 50 at.% Ni solid solutions, from which the NTC

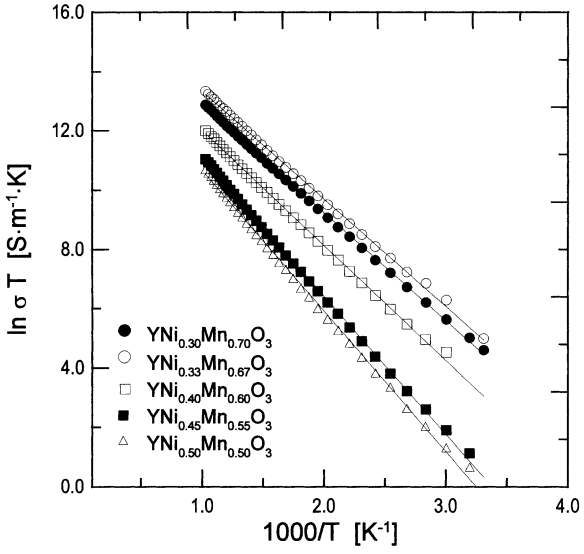

Fig. 5. Log σT vs $1/T$ for different compositions.

Table 2
Electrical conductivity at 20 and 700°C and activation energy for the perovskite solid solution as a function of the Ni amount

% Ni	30	33	40	45	50
σ (Sm^{-1}) 20°C	2.83×10^{-1}	4.68×10^{-1}	7.2×10^{-1}	4.50×10^{-3}	2.40×10^{-3}
σ (Sm^{-1}) 700°C	403	629	165	63	42
E_a (eV)	0.27	0.27	0.29	0.35	0.36

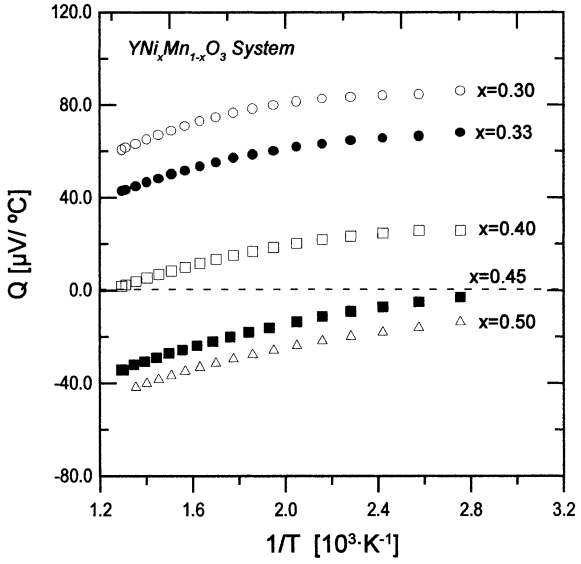

Fig. 6. Seebeck coefficient vs temperature for different solid solutions.

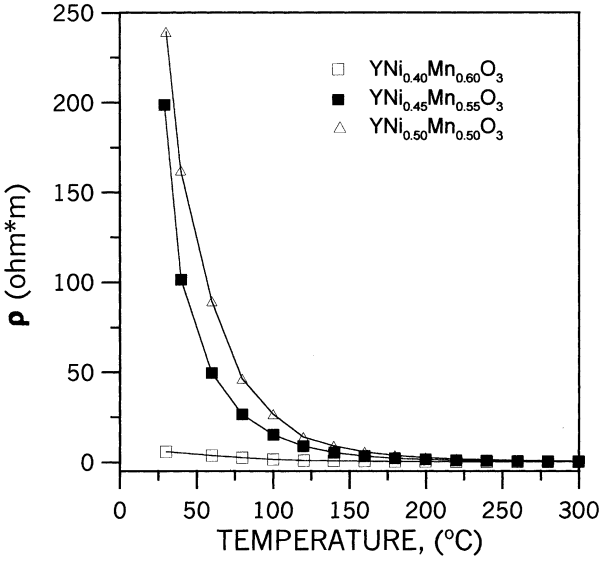

Fig. 7. Resistivity vs temperature curves for compositions with $x \geqslant 0.40$.

Table 3
NTC characteristics parameters of solid solutions $YNi_xMn_{1-x}O_3$

Compositions	ρ (Ω*m), at 20°C	B (K)	α (%/K), at 20°C
$YNi_{0.40}Mn_{0.60}O_3$	14	3360	−3.91
$YNi_{0.45}Mn_{0.55}O_3$	230	4150	−4.83
$YNi_{0.50}Mn_{0.50}O_3$	420	4260	−4.96

parameters have been calculated. The curves show a typical behaviour of NTC thermistors. Table 3 shows the calculated parameters. As it can be seen, all three compositions show a good negative temperature coefficient. The samples corresponding to 45 and 50 at.% Ni have B values higher than 4000, and α values $<$-4%/K, which make these ceramic materials very interesting for NTC applications, when they are compared with commercial compositions.[16]

Reaction mechanisms between yttrium nickel manganites and yttria-sustituted ceria and yttria-stabilised zirconia have been performed for establishing the feasibility of these manganites as ceramic electrode for use in SOFCs. The manganite has proven to be compatible with Y-sustituted ceria solid solutions, whereas the Y-fully stabilised zirconia reacts with the manganite, with a strong degradation of the perovskite structure. More detailed work will be published elsewhere.[17]

4. Conclusions

The substitution of Ni^{2+} for Mn^{3+} in the hexagonal $YMnO_3$ compound leads to a phase transition from hexagonal phase to an orthorhombic, perovskite-type phase for Ni amounts below 20 at.%, in a similar manner to that reported for the (Y,Ca)MnO_3 solid solutions. The reason for this transition seems to be related to the decrease of the Mn^{3+} Jahn–Teller cations concentration in the lattice.

Above 50 at.% Ni a two-phase region has been observed, and unreacted Y_2O_3 is detected. In this system the nickel cation seems to be unable to adopt the three-valent state which would be necessary to incorporate in the B lattice sites of the perovskite structure, maintaining their stability and stoichiometry.

The perovskite-type solid solutions, ($x = 0.25-0.50$) are semiconducting materials. They show good electrical conductivity values, and promising NTC features. The conductivity at 700°C of solid solutions in the Mn-rich region is high enough for use in SOFCs.

Acknowledgements

This work was supported by Spain CICYT-MAT-97-0679-C02-01

References

1. Hammouche, A., Siebert, E. and Hammou, A., Crystallographic, thermal and electrochemical properties of the system $La_{1-x}Sr_xMnO_3$ for high temperature solid oxide fuel cells. *Mater. Res. Bull.,* 1989, **24**, 367–380.
2. Tanaka, J., Takahashi, K., Yukino, K. and Horiuchi, S., Electrical conduction of $(La_{0.8}Ca_{0.2})MnO_3$ with homogeneous ionic distribution. *Phys. Status Solidi,* 1983, **80**, 621–630.
3. Ostergard, M. J. L. and Mogensen, M., AC impedance study of the oxygen reduction mechanism on $La_xSr_{1-x}MnO_3$ in SOFC. *Electrochimica Acta,* 1993, **38**, 2015–2020.
4. Urishabara, A., Moritomo, Y., Arima, T., Asatmisu, A., Kido, G. and Yokura, Y., Insulator–metal transition and giant magnetoresistance in $La_{1mx}Sr_xMnO_3$. *Phys. Rev. B*, 1995-II, 51, **14**, 103–109.
5. Muller, O. and Roy, R., *The Major Ternary Structural Families*. Springer Verlag, New York, 1974.
6. Yakel, H. L., Koehler, W. C., Bertaut, E. F. and Forrat, E. F., On the crystal structure of the manganese(III) trioxides of the heavy lanthanides and yttrium. *Acta Crystallogr.,* 1963, **16**, 957–962.
7. Coure, Ph., Guinet, Ph., Peuzin, J., Buisson, G. and Bertaut, E. F., Ferroelectric properties of hexagonal orthomanganites of yttrium and rare earths. *Proc. Int. Meeting Ferroelectricity,* 1966, **V**, 332–340.
8. Moure, C., Fernandez, J. F., Villegas, M. and Duran, P., Non-ohmic behaviour and switching phenomena in $YMnO_3$-based ceramic materials. *J. Eur. Ceram. Soc.,* 1999, **19**, 131–137.
9. Moure, C., Fernandez, J. F., Villegas, M., Tartaj, J. M. and Duran, P., Phase transition and electrical conductivity in the system $YmnO_3$–$CaMnO_3$. *J. Mater. Sci.,* 1999, **94**, 2565–2568.
10. Heikes, R. and Ure, R., *Thermoelectricity: Science and Engineering*. Interscience Publishers, New York, 1961.
11. Shannon, R. D., Revised effective ionic radii and systematic studies of interatomic distanced in halides and chalcogenides. *Acta Crystallogr.,* 1976, **A32**, 751–767.
12. Moure, C., Gutierrez, D., Fernandez, J. F., Tartaj, J., Duran, P. and Pena, O., Phase transitions induced on hexagonal manganites by the incorporation of aliovalent cations on a or b sites. *Bol. Soc. Esp. Ceram. Vidr.,* 1999, **38**, 417–420.
13. Yamamoto, O., Takeda, Y., Kanno, R. and Noda, M., Perovskite-type oxides as oxygen electrodes for high temperature oxide fuel cells. *Solid State Ionics,* 1987, **22**, 241–246.
14. Clarke, D. R., Shaw, T. M. and Dimos, D., Issues in the processing of cuprate ceramic superconductors. *J. Am. Ceram. Soc.,* 1989, **72**, 1103–1113.
15. Subba Rao, G. V., Wanklyn, B. M. and Rao, C. N. R., Electrical transpor in rare-earth ortho-chromites,-manganites and ferrites. *J. Phys. Chem. Solids,* 1971, **32**, 345–358.
16. Moulson, A. J. and Herbert, J. M., *Electroceramics, Materials, Properties, Aplications*. Chapman and Hall, London, 1990.
17. Moure, C., Gutierrez, D., Tartaj, J., Capel, F., Duran, P., Reaction mechanisms between yttrium nickel manganite and yttria-doped ceria and zirconia.